Environmental Science & Technology

pubs.acs.org/est

Article

Iron-Facilitated Organic Radical Formation from Secondary Organic Aerosols in Surrogate Lung Fluid

Jinlai Wei, Ting Fang, Pascale S. J. Lakey, and Manabu Shiraiwa*

Cite This: https://doi.org/10.1021/acs.est.1c04334

Read Online

ACCESS | Metrics & More | Article Recommendations | Supporting Information

ABSTRACT: Respiratory deposition of secondary organic aerosols (SOA) and iron may lead to the generation of reactive oxygen species and free radicals in lung fluid to cause oxidative stress, but their underlying mechanism and formation kinetics are not well understood. Here we demonstrate substantial formation of organic radicals in surrogate lung fluid (SLF) by mixtures of Fe^{2+} and SOA generated from photooxidation of isoprene, α-terpineol, and toluene. The molar yields of organic radicals by SOA are measured to be 0.03−0.5% in SLF, which are 5−10 times higher than in water. We observe that Fe^{2+} enhances organic radical yields dramatically by a factor of 20−80, which can be attributed to Fe^{2+}-facilitated decomposition of organic peroxides, in consistency with a positive correlation between peroxide contents and organic radical yields. Ascorbate mediates redox cycling of iron ions to sustain organic peroxide decomposition, as supported by kinetic modeling reproducing time- and concentration-dependence of organic radical formation as well as additional experiments observing the formation of Fe^{2+} and ascorbate radicals in mixtures of ascorbate and Fe^{3+}. $^{\bullet}OH$ and superoxide are found to be scavenged by antioxidants efficiently. These findings have implications on the role of organic radicals in oxidative damage and lipid peroxidation.

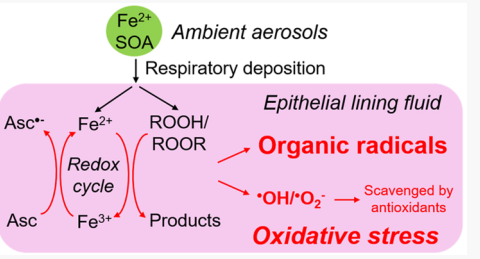

KEYWORDS: *SOA, iron, organic radicals, reactive oxygen species, lung fluid, oxidative stress*

INTRODUCTION

Secondary organic aerosols (SOA) represent a substantial fraction of ambient particulate matter (PM) and play a significant role in air quality and public health.[1−3] SOA are generated from oxidation of anthropogenic and biogenic volatile organic compounds (VOCs) followed by nucleation and condensation of semi- and low-volatile oxidation products.[4] Transition metals are also important for aerosol health effects and iron is regarded as being especially important due to its strong redox activity. Iron is emitted from anthropogenic and crustal sources such as diesel emissions, nonexhaust emissions, and resuspension of dust.[5,6] In atmospheric aerosol particles the water-soluble fractions of iron are reported to be up to about 20%[7,8] with majority (>60%) in the form of Fe (III), while significantly greater fractions (up to 90%) of Fe (II) can be found in fog and cloud water.[8,9] Mineral dust can take up organic compounds to facilitate particle formation and growth and to become internally mixed with organics.[10−12]

Inhalation and respiratory deposition of redox-active PM components can lead to the formation of reactive oxygen species including hydroxyl radicals ($^{\bullet}OH$), superoxide/hydroperoxyl radicals ($O_2^{\bullet-}/HO_2^{\bullet}$), hydrogen peroxide ($H_2O_2$) and organic radicals, which may cause oxidative stress. PM oxidative potential is related to ROS formation and it has been suggested to be an emerging indicator of aerosol health effects in addition to PM mass concentrations.[13−15] While substantial efforts have been made to advance our understanding of toxicity and oxidative potential of SOA and metals, the underlying mechanism of oxidative stress and linkage to ROS formation by PM in lung fluid are still poorly established.[3]

SOA contain a number of oxidized products such as alcohols, carboxylic acids, and highly oxygenated organic molecules (HOMs) with multiple peroxide functionalities.[16−18] Organic hydroperoxides[19,20] and peracids[21] can decompose to form $^{\bullet}OH$, which can be enhanced with Fenton-like interactions of ferrous ion.[19,22] Subsequent $^{\bullet}OH$ oxidation of primary or secondary alcohols can lead to the formation of $O_2^{\bullet-}/HO_2^{\bullet}$.[23] A very recent study demonstrated the formation and stabilization of carbon-centered radicals in organic aerosols containing Fe ions.[24] Despite recent progress, the chemical mechanism of ROS formation induced by SOA and transition metals is highly uncertain, especially in lung fluid.

In this study, we characterized radical formation from laboratory-generated SOA and Fe^{2+} in water and in surrogate lung fluid (SLF). We observed major formation of $^{\bullet}OH$ and

Special Issue: Urban Air Pollution and Human Health

Received: June 30, 2021
Revised: August 20, 2021
Accepted: September 21, 2021

$O_2^{\bullet-}/HO_2^{\bullet}$ in water, but dominant formation of organic radicals in SLF with significant enhancement effects by Fe^{2+}. Kinetic modeling elucidated that the substantial formation of organic radicals is due to Fe^{2+}-facilitated decomposition of organic peroxides and subsequent aqueous reactions, which is further enhanced by antioxidants through Fe^{3+}/Fe^{2+} redox cycling. We found that $^{\bullet}OH$ and $O_2^{\bullet-}/HO_2^{\bullet}$ can be effectively scavenged by lung antioxidants, while some organic radicals can persist due to relatively longer lifetimes and low reactivity with antioxidants. This work provides the mechanistic explanation for organic radical formation in lung fluid by SOA and Fe^{2+} with significant implications on oxidative stress.

MATERIALS AND METHODS

SOA Formation, Collection, and Extraction. SOA particles were generated from $^{\bullet}OH$ photooxidation of isoprene (Sigma-Aldrich, ≥99%), α-terpineol (Arcos Organics, ≥97%), and toluene (Alfa Aesar, ≥99.7%) using a potential aerosol mass (PAM) reactor.[25] We selected isoprene and toluene because they are among the most heavily emitted biogenic[26] and anthropogenic[27] VOCs, respectively. α-Terpineol was selected as an important biogenic and indoor-relevant VOC, which is a significant component of liquid cleaner/disinfectants and air fresheners.[28] Detailed procedures of SOA formation can be found in our recent study.[23] Despite high $^{\bullet}OH$ concentrations (~10^{10} cm^{-3}) compared to ambient levels (~10^{6} cm^{-3}), previous studies have shown that the PAM reactor can generate SOA highly relevant to that from ambient and chamber conditions in terms of mass yield, oxidation state, hygroscopicity, and chemical composition with similar mass spectra measured by an Aerodyne ToF AMS.[29−31] Additional advantages of the PAM reactor include efficient generation of SOA mass in shortened experimental time scales, ability to reach long photochemical ages, and minimized wall losses.[31−33] Nevertheless, the lifetimes of peroxy radicals in the PAM reactor are much shorter compared to typical ambient conditions and the reaction regime with high radical concentrations would affect SOA chemistry;[31] thus, future studies with ambient SOA or SOA generated with low concentrations would be warranted.

A scanning mobility particle sizer (SMPS, Grimm Aerosol Technik) was used to monitor the number concentrations and size distributions of PAM-generated SOA. Particle sampling was initiated after the number concentrations stabilized. The SOA particles were collected on 47 mm polytetrafluoroethylene (PTFE) filters (Millipore FGLP04700, 0.2 μm pore size) for 30−60 min with average mass loadings of 0.35 ± 0.06 mg, 2.18 ± 0.15 mg, and 1.04 ± 0.16 mg for isoprene, toluene, and α-terpineol SOA, respectively. The filter samples were extracted in 1 mL spin-trap solution (10 mM) containing Fe^{2+} salt ($(NH_4)_2Fe(SO_4)_2$, Sigma-Aldrich, 99%, 0−0.8 mM) in water or in buffered SLF (pH 7.4). SLF is an artificial solution containing naturally occurring lung antioxidants including L-ascorbic acid (Asc, 200 μM, Sigma-Aldrich, 99%), L-glutathione reduced (GSH, 100 μM, Sigma-Aldrich, >98%) and uric acid (100 μM, UA, Sigma-Aldrich, >99%).[34] It also contains citric acid (CA, 300 μM, Sigma-Aldrich, >99.5%), mimicking metal-binding proteins *in vivo*.[35] A phosphate buffer saline (PBS, Corning, 10×) was used to maintain the physiological pH at 7.4 in SLF. The mass difference before and after the extraction was regarded as the amount of SOA dissolved in reagents, and an average molar mass of 200 g mol^{-1} was assumed for the calculation of SOA molar concentrations in filter extracts. SOA concentrations were in the range of 1.2−2.1 mM, 2.0−3.9 mM and 5.6−9.9 mM for isoprene, α-terpineol, and toluene SOA, respectively. The pH of the SOA extracts in water varied between 4 and 6. Two SOA samples were prepared for each Fe^{2+} concentration for the analysis of radical formation. More detailed procedures of SOA formation, collection and extraction can be found in our previous study.[23]

Experiments were also conducted using the model compounds of ROOR and ROOH including *tert*-butyl peroxybenzoate (Sigma-Aldrich, 98%), *tert*-butyl peracetate (Sigma-Aldirch, 50 wt %), cumene hydroperoxide (Alfa Aesar, 80%), benzoyl peroxide (Sigma-Aldrich, ≥98%), and dicumyl peroxide (Sigma-Aldrich, 98%). 0.1 mM Fe^{2+} and 10 mM peroxides were mixed with 10 mM BMPO in water and SLF, respectively, followed by EPR measurements.

EPR Measurements. A continuous-wave electron paramagnetic resonance (CW-EPR) spectrometer (Bruker, Germany) coupled with a spin-trapping technique was used for free radical quantification. The spin-trapping agent 5-*tert*-Butoxycarbonyl-5-methyl-1-pyrroline-*N*-oxide (BMPO) (Enzo, ≥99%) was used to capture free radicals generated upon aqueous reactions of SOA. After particle extraction from a filter, the extracts were incubated at a room temperature of 20 °C. A 50 μL aliquot was loaded into a 50 μL capillary tube (VWR) and inserted in the resonator of the EPR spectrometer at 10, 20, 60, 120, 180, and 240 min from the start of aqueous reactions. The parameters for EPR measurements are as follows: a center field of 3515.0 G, a sweep width of 100.0 G, a receiver gain of 30 dB, a modulation amplitude of 1.0 G, a scan number of 10−50, attenuation of 12 dB, a microwave power of 12.6 mW, a modulation frequency of 100 kHz, a microwave frequency of 9.86 GHz, and a conversion time and time constant of 5.12 ms. After obtaining the EPR spectra, SpinFit and SpinCount methods embedded in the Bruker Xenon software were applied to quantify BMPO−radical adducts[19] at each time point. Consistent with our previous study,[23] the detection limits for all BMPO−radical adducts are around 50−80 nM. The radical yield was calculated by normalizing the concentrations of BMPO adducts with SOA concentrations in the aqueous extracts.

Fe^{2+} Measurement. Fe^{2+} measurements were performed using the ferrozine method.[36] The stock solution of 2.55 mg/mL ferrozine (3-(2-pyridyl)-5,6-diphenyl-1,2,4-triazine-p,p′-disulfonic acid monosodium salt hydrate, Sigma-Aldrich, 97%) was prepared. We added 100 μL of this solution to 10 mL samples containing Fe^{3+} or Fe^{3+} + ascorbate, and the magenta-colored ligand formed by Fe^{2+} and ferrozine was quantified by an online miniature spectrophotometer (Ocean Optics) at a characteristic wavelength of 562 nm. The calibration was conducted using Fe^{2+} standard solutions (Supporting Information (SI) Figure S1). Note that the control experiments show that Fe^{3+} or ascorbate alone with ferrozine do not generate Fe^{2+} signal above detection limit (4 nM).

Total Peroxide Measurement. The total peroxide measurements were conducted using a modified iodometric-spectrophotometric method.[37] Peroxides in all forms (ROOH, ROOR, HOOH) can oxidize I^- to form I_2, which combines with the excess I^- to form I_3^- with characteristic absorbance peaks at wavelengths 289 and 350 nm[38] and the absorbance at 350 nm was measured in this study. Isoprene, α-terpineol and toluene SOA were extracted in 1 mL Milli-Q water for 7 min,

https://doi.org/10.1021/acs.est.1c04334
Environ. Sci. Technol. XXXX, XXX, XXX−XXX

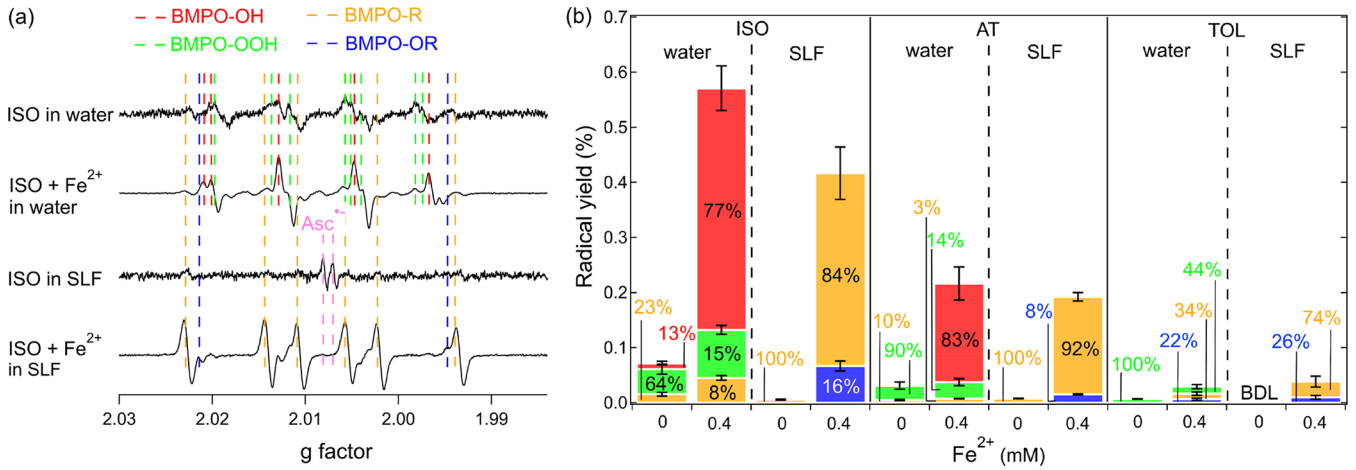

Figure 1. (a) EPR spectra of isoprene SOA with 0 or 0.4 mM Fe^{2+} in water and SLF in the presence of spin-trapping agent BMPO. The dashed vertical lines represent different BMPO−radical adducts and ascorbate radicals ($Asc^{\bullet-}$). (b) Yields and relative abundance of different radical species including BMPO−OH (red), BMPO−OOH (green), BMPO−R (yellow) and BMPO−OR (blue) from isoprene (ISO), α-terpineol (AT), and toluene (TOL) SOA in water and SLF with 0 or 0.4 mM Fe^{2+}. Radical yields peaked and thus selected to show at reaction time of 20 min in water and 60 min in SLF, respectively. The error bars represent the error propagation from the two duplicates in EPR measurement and the uncertainty in SOA mass measurements.

after which 100 μL of the SOA extracts were mixed with 700 μL ethyl acetate (Sigma-Aldrich, 99.8%) to obtain 800 μL diluted extracts. Then the 800 μL diluted extracts were mixed with 1200 μL reagents consisting of 636 μL acetic acid (Sigma-Aldrich, ≥99%), 324 μL chloroform (Sigma-Aldrich, ≥99.5%) and 240 μL water (acetic acid/chlroform/water = v/v 0.53:0.27:0.20). Note that the dilution factor of SOA extracts in the reagents (i.e., 100 μL in 2000 μL) was determined when different reagents were completely miscible so that the solution was homogeneous. The 2000 μL diluted SOA extracts with reagents were then purged with a flow of 15 ccm N_2 for 1 min to exclude dissolved oxygen that can also oxidize I^-. Next, 20 mg of potassium iodide (KI, Sigma-Aldrich, ≥99%) was added into each sample, after which the vials were capped and allowed to stand for 1 h. Lastly, the solution was further diluted in water by a factor of 200 (25 μL in 5000 μL) and the absorbance at 350 nm was measured using an online miniature spectrophotometer (Ocean Optics). The calibration was performed using 0.2−2 μM benzoyl peroxide (Sigma-Aldrich, ≥98%) and the calibration curve is shown in SI Figure S2. Blank (water instead of SOA extracts or benzoyl peroxide) correction was always performed and the measurements were repeated twice for each SOA sample.

DTT Assay. The dithiothreitol (DTT) assay was performed following the protocol in Fang et al.[39] Briefly, the consumption rate of DTT is considered as an indicator of the oxidative potential. To perform this assay, a 1 mL reaction vial was prepared consisting of 0.7 mL samples or blank, 0.2 mL phosphate buffer (0.5 M KH_2PO_4 and K_2HPO_4, Sigma-Aldrich) and 0.1 mL of 1 mM DTT (Sigma-Aldrich, ≥99%). The reaction starts with the addition of DTT, and a 100 μL aliquot was withdrawn from the reaction vial at 0, 5, 10, 15, and 20 min and added to 1 mL of TCA (trichloroacetic acid, LabChem, 1% w/v) to quench the reaction. The reaction vials were incubated at 37 °C in a thermo mixer (Eppendorf). Next, 2 mL Tris buffer (0.08 M Trizma base, Sigma-Aldrich, ≥ 99.9% with pH adjusted to 8.9 by hydrochloric acid (LabChem, 10 M)) and 0.5 mL DTNB (0.2 mM, 5,5′-dithiobis(2-nitrobenzoic acid, Sigma-Aldrich, ≥ 98%) were added to the quenched aliquot. The mixture was then diluted 10 times and immediately measured by the absorbance of 412 nm using an online miniature spectrophotometer (Ocean Optics). Note, a blank control (Milli-Q water) was always performed in each experiment. For the SOA extracts, isoprene and α-terpineol SOA were diluted 10 times, while toluene SOA was diluted 20 times to obtain linear DTT consumption rate within the time scale of the experiment. The $[Fe^{2+}]/[SOA]$ molar ratios in the reaction vials were maintained consistent with those in EPR measurement.

Kinetic Modeling. A kinetic model was applied to simulate the radical formation by aqueous reactions of isoprene SOA with Fe^{2+} in SLF using the reactions listed in SI Table S1. The reactions include radical chemistry involving SOA (R1−R31), ROS coupling (R32−R41), reactions of Fe ions (R42−R51), reactions involving antioxidants (R52−R63), and BMPO chemistry (R64−R84). The mechanisms of $^{\bullet}OH$ and $^{\bullet}O_2^-/HO_2^{\bullet}$ formation from SOA (R1, R3, and R4) were explicitly addressed in our previous study,[23] with the addition of Fe^{2+}-catalyzed ROOH decomposition (R2).[19,40] The $RO^{\bullet}$ formation originates from Fe^{2+}-catalyzed decomposition of ROOR (R5) and ROOH (R10, branching of R2), which can be further converted to $R^{\bullet}$ through isomerization (R12),[41] decomposition (R13),[42] and bimolecular reactions (R14−R16).[43] Note that the rate coefficients involving SOA chemistry were assumed to be independent of the structures of R groups contained in isoprene SOA, representing a major model assumption. The variations in rate coefficients depending on R structures were reflected in the uncertainties shown in SI Table S1.

The rate coefficients of ROS coupling reactions were obtained from literature values. For Fe-oxidant interaction (R42−R45), we also consider potential impacts of Fe-citrate ligand on the rate coefficients as demonstrated by Gonzalez et al.[44] The rate coefficients of antioxidants with radicals and Fe ions were also adopted from literature, except that the scavenging of $R^{\bullet}$ and $RO^{\bullet}$ by ascorbate (R56 and R57) were assumed to be a few orders of magnitude slower than that of $^{\bullet}OH$ and $^{\bullet}O_2^-/HO_2^{\bullet}$ (R52 and R55). This is in line with the experimental results showing BMPO−OH and BMPO−OOH below the detection limit, in contrast to the significant

https://doi.org/10.1021/acs.est.1c04334
Environ. Sci. Technol. XXXX, XXX, XXX−XXX

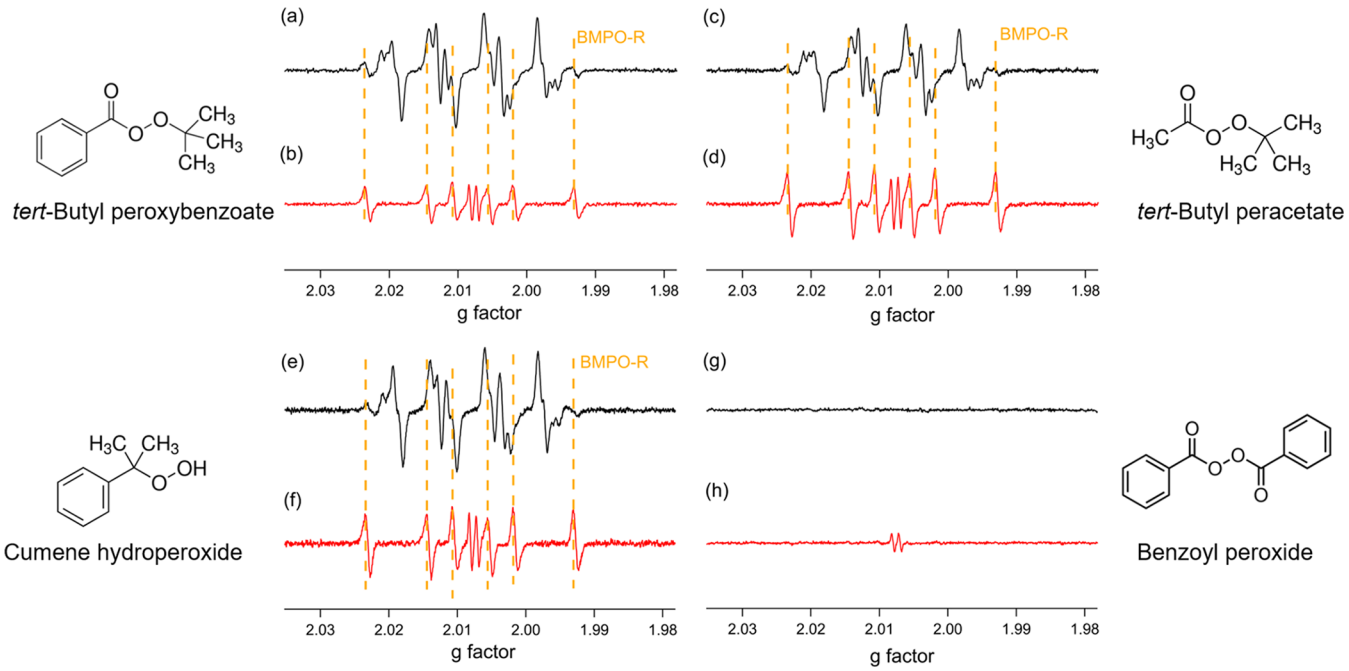

Figure 2. EPR spectra of mixtures of 0.1 mM Fe^{2+} with 10 mM (a,b) *tert*-butyl peroxybenzoate, (c,d) *tert*-butyl peracetate, (e,f) cumene hydroperoxide, and (g,h) benzoyl peroxide in water (black) or SLF (red).

formation of BMPO−R and BMPO−OR in SLF. The redox cycling of Fe^{3+}/Fe^{2+} by ascorbate is also considered (R63). The unknown rate coefficients and molar fractions of ROOH, R_1R_2CHOH and ROOR contained in isoprene SOA were determined using the Monte Carlo genetic algorithm (MCGA) to reproduce experimental data.[45] In the Monte Carlo search, input parameters were varied randomly within individual bounds: the boundaries of all reaction rate constants were generally constrained to within 2 or 3 orders of magnitude based on literature values, whereas the ROOH/R_1R_2CHOH/ROOR molar fractions were constrained to between 0.1% and 80%. The uncertainty of the rate coefficients in SI Table S1 and the ROOH/R_1R_2CHOH/ROOR fractions in SI Table S2 were obtained by running the MCGA numerous times (>100), among which 40 parameter sets were selected which reasonably captured the temporal trends of the experimental data.

RESULTS AND DISCUSSION

Radical Formation from SOA and Fe^{2+} in Water and SLF. Figure 1a shows the observed EPR spectra of isoprene SOA in water and SLF in the absence of Fe^{2+} or in the presence of 0.4 mM Fe^{2+}. The simulations and deconvolution of EPR spectra (SI Figure S3) allow us to quantify the absolute radical yields and relative abundance of different types of BMPO radical adducts including $^{\bullet}OH$, $O_2^{\bullet-}/HO_2^{\bullet}$, and carbon- and oxygen-centered organic radicals. As shown in Figure 1b, we find striking enhancements in the observed total radical yields with Fe^{2+} addition in both water (from 0.07% to 0.57%) and SLF (from 0.005% to 0.42%) with large changes in radical composition. Isoprene SOA in water leads to the predominant formation of superoxide (64%) with a minor contribution from $^{\bullet}OH$ and carbon-centered radicals; upon the addition of 0.4 mM Fe^{2+}, the radical profile becomes dominated by $^{\bullet}OH$ (77%) with contributions from $O_2^{\bullet-}/HO_2^{\bullet}$ (15%) and carbon-centered radicals (8%) (Figure 1b). In the presence of antioxidants in SLF without Fe^{2+}, only carbon-centered radicals are observed, while a minor contribution from oxygen-centered organic radicals (16%) is also observed with 0.4 mM Fe^{2+}. $^{\bullet}OH$ and $O_2^{\bullet-}/HO_2^{\bullet}$ radicals are not observed in SLF, indicating effective scavenging of these highly reactive species by antioxidants, which is consistent with the formation of ascorbate radicals ($Asc^{\bullet-}$)[46] in Figure 1a. Note that the detected organic radical formation in SLF should be attributed to isoprene SOA with negligible contributions from $Asc^{\bullet-}$ trapping by BMPO, as $^{\bullet}OH$ radicals formed by the Fenton reaction (Fe^{2+} + H_2O_2) are effectively scavenged in the SLF by ascorbate forming $Asc^{\bullet-}$ without the formation of organic radical adducts (SI Figure S4).

In addition to isoprene SOA, α-terpineol and toluene SOA are also characterized for the radical yields in water and SLF, with the observed EPR spectra shown in SI Figure S5. In water, α-terpineol and toluene SOA alone consistently generate radicals dominated by $O_2^{\bullet-}/HO_2^{\bullet}$ (>90%). The total radical yields are elevated by a factor of 4−8 upon Fe^{2+} addition: α-terpineol SOA exhibits dominant (83%) $^{\bullet}OH$ formation which is similar to isoprene SOA (77%), while we observe no $^{\bullet}OH$ above the detection limit from toluene SOA + Fe^{2+} in water. In SLF, Figure 1b shows consistent enhancement effects by Fe^{2+} in organic radical formation, with radical yields increasing substantially from 0.008% to 0.19% for α-terpineol SOA and from below the detection limit (BDL) to 0.04% for toluene SOA, respectively. Carbon-centered radicals are the dominant species for α-terpineol (92%) and toluene (74%) SOA with minor contributions from oxygen-centered organic radicals (8% and 26%, respectively). Overall, we observe the highest radical yields and strongest enhancement effects of Fe^{2+} (by a factor up to ~80) from isoprene SOA followed by α-terpineol and toluene SOA.

Reaction Mechanisms. To elucidate the chemical mechanisms of organic radical formation by SOA and Fe^{2+}, we developed and applied a kinetic model to simulate the temporal evolution of $R^{\bullet}$ and $RO^{\bullet}$ radicals. The following

https://doi.org/10.1021/acs.est.1c04334
Environ. Sci. Technol. XXXX, XXX, XXX−XXX

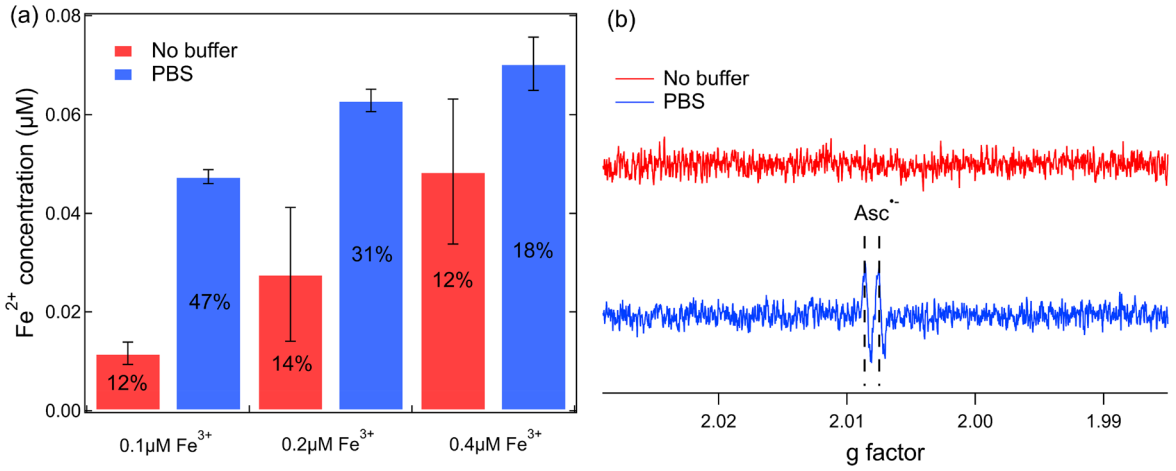

Figure 3. (a) Concentrations of Fe^{2+} formed in the mixtures of ascorbate (10 μM) with Fe^{3+} (0.1, 0.2, and 0.4 μM) with and without PBS. The number on each bar represents the percentage of Fe^{3+} that gets reduced by ascorbate. (b) EPR spectra of 0.1 mM Fe^{3+} and 0.2 mM ascorbate with and without PBS. The pH is 4−5 without PBS in the mixtures.

reactions were implemented into the kinetic model for radical formation from isoprene SOA and Fe^{2+} based on previous studies:

$$ROOH \rightarrow RO^{\bullet} + {}^{\bullet}OH \quad (R1)$$

$$ROOH + Fe^{2+} \rightarrow RO^{-} + {}^{\bullet}OH + Fe^{3+} \quad (R2)$$

$$R_1R_2CHOH + {}^{\bullet}OH \xrightarrow{O_2} c_1R_1R_2C(O_2)OH^{\bullet} \quad (R3)$$

$$R_1R_2C(O_2)OH^{\bullet} \rightarrow R_1C(O)R_2 + HO_2^{\bullet} \quad (R4)$$

$$ROOR' + Fe^{2+} \rightarrow RO^{\bullet} + R'O^{-} + Fe^{3+} \quad (R5)$$

SOA contain organic hydroperoxides (ROOH), which can undergo thermal decomposition to yield $^{\bullet}OH$ radicals (R1), which can be drastically promoted by Fe^{2+} with the Fenton-like reaction leading to enhanced formation of $^{\bullet}OH$ (R2).[19] Note that R1 occurs for ROOH without additional functionalities on the α-carbon, as the decomposition of α-hydroxyhydroperoxides leads to the formation of carbonyl and H_2O_2.[47,48] $HO_2^{\bullet}$ is formed subsequently by $^{\bullet}OH$ oxidation of primary or secondary alcohols (R_1R_2CHOH) followed by fast addition of dissolved oxygen (R3) and unimolecular decomposition of α-hydroxyperoxyl radicals (R4).[49] Our recent study showed that this mechanism can explain the dominated $O_2^{\bullet-}/HO_2^{\bullet}$ formation from the aqueous reactions of isoprene and terpene SOA in the absence of Fe^{2+}.[23] While organic peroxides (ROOR') are thermally stable, they are known to be reactive toward Fe^{2+}, releasing $RO^{\bullet}$ radicals (R5) in analogy to R2.[50,51]

To confirm Fe^{2+}-facilitated decomposition of organic peroxides, we measured radical formation in mixtures of Fe^{2+} and commercially available organic hydroperoxides and peroxides in water and SLF. As shown in Figure 2, *tert*-butyl peroxybenzoate, *tert*-butyl peracetate (ROOR), and cumene hydroperoxide (ROOH) produce various radicals via Fenton-like reactions of Fe^{2+} in water; note that organic radicals are below detection limit without Fe^{2+}. Benzoyl peroxide and dicumyl peroxide (not shown) are found to be unreactive with Fe^{2+} within the time scale of our experiments, indicating that some organic peroxides are very stable. In SLF, only $R^{\bullet}$ was formed and other radicals ($^{\bullet}OH$, $O_2^{\bullet-}$, $RO^{\bullet}$) were hardly observed. It indicates efficient scavenging of reactive radicals by antioxidants and rapid conversion of $RO^{\bullet}$ to $R^{\bullet}$.

Indeed, we observed significantly higher formation of $R^{\bullet}$ than $RO^{\bullet}$ from isoprene SOA in both water and SLF (Figure 1b), most likely due to the rapid conversion of $RO^{\bullet}$ to $R^{\bullet}$ via isomerization (R12 in Table S1), decomposition (R13) and a bimolecular reaction resulting in H abstraction (R14).[52] While the isomerization and decomposition of $RO^{\bullet}$ are established in the gas phase, these pathways can also occur in the aqueous phase.[53] Our model sensitivity analysis suggested that R12 and R13 contribute to over 99% of the total BMPO−R formation, consistent with Carrasquillo et al.[43] showing that a bimolecular reaction as a negligible channel in the condensed phase. Isomerization and decomposition rates of $RO^{\bullet}$ are comparable in forming $R^{\bullet}$ given the fitted rate coefficients ($(0.05-6.4) \times 10^6$ s^{-1} and $(0.1-9.6) \times 10^5$ s^{-1}, respectively), which are in line with literature values ($<10^7$ s^{-1}[41] and $<1.4 \times 10^6$ s^{-1},[42] respectively).

The significantly higher formation of organic radicals in SLF than in water can be attributed to redox cycling of Fe^{3+}/Fe^{2+} mediated by antioxidants (R63): $Fe^{3+} + AscH^{-} \rightarrow Fe^{2+} + H^{+} + Asc^{\bullet-}$. Fe^{3+} can be reduced rapidly to regenerate Fe^{2+} by ascorbate anions,[54−57] maintaining reaction rates of R5 and R10 to sustain organic radical formation. The model sensitivity analysis revealed that such recycling of Fe^{2+} contribute to 5−10 times higher organic radical formation in the SLF than in water. Note that a very recent study suggested that Fe^{3+} and ascorbate reactions are catalytic rather than redox reactions:[58] $Fe^{3+} + Asc + O_2 \rightarrow Fe^{3+} +$ dehydroascorbic acid (DHA) + H_2O_2. To further investigate the nature of the Fe^{3+}-ascorbate reaction, we measured Fe^{2+} in the mixtures of Fe^{3+} and ascorbate in water or PBS solutions. Figure 3a shows that 12−14% of Fe^{3+} can be reduced to form Fe^{2+} in water, which can be further enhanced when buffered by PBS (18−47%). In addition, EPR measurements show that $Asc^{\bullet-}$ is formed in the Fe^{3+}-Asc mixtures when buffered by PBS (Figure 3b), which is only generated by redox instead of catalytic reactions. Interestingly, both Fe^{2+} and $Asc^{\bullet-}$ measurements indicate that Fe^{3+}-Asc redox reactions are highly pH-dependent and more prominent when buffered by PBS. We also conducted sensitive analysis in the model, showing that the redox reactions remain the dominant channel of Fe^{3+}-Asc interaction even if the catalytic reactions are considered (see details in SI). Future studies are required to elucidate the relative importance

https://doi.org/10.1021/acs.est.1c04334
Environ. Sci. Technol. XXXX, XXX, XXX−XXX

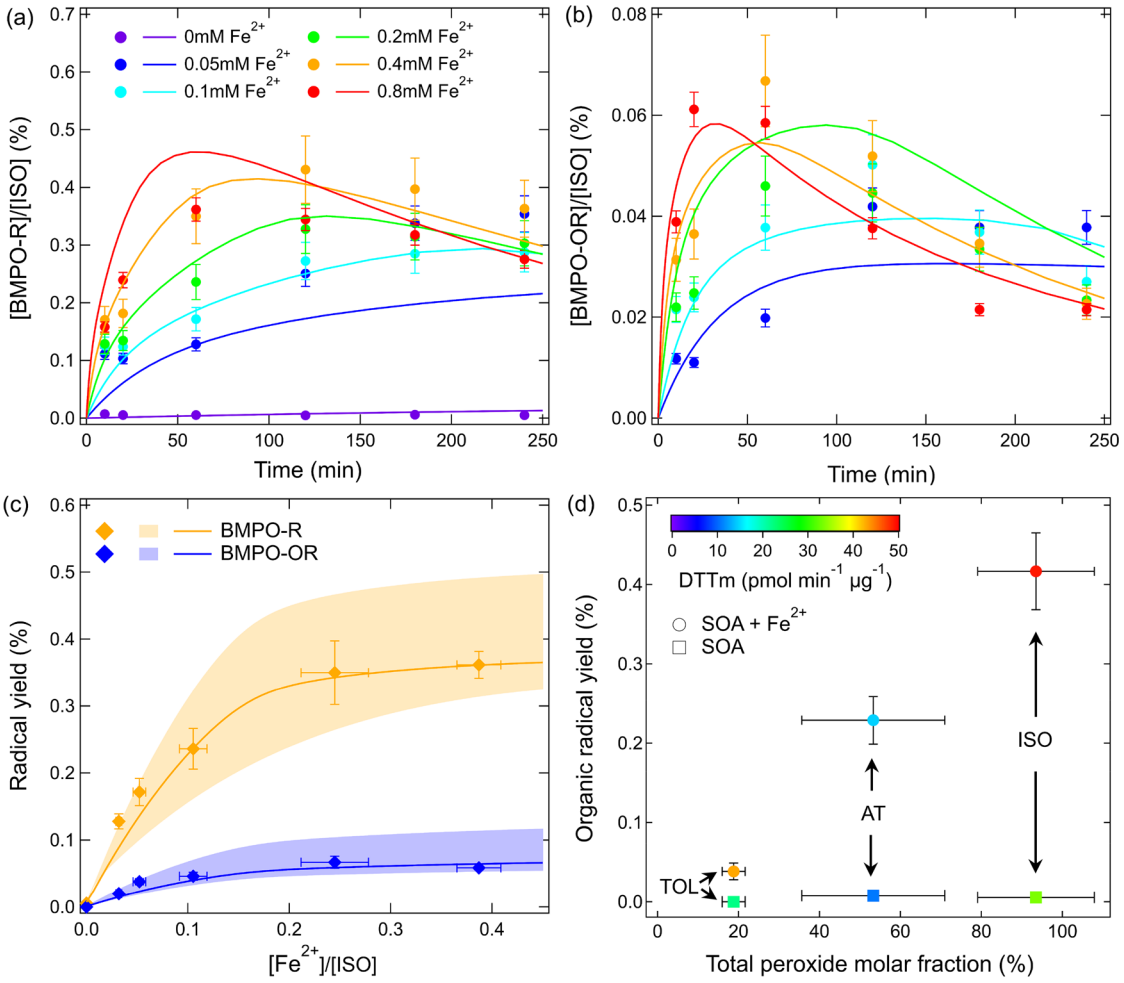

Figure 4. (a) Temporal evolution of molar yields of (a) BMPO−R and (b) BMPO−OR from aqueous reactions of isoprene SOA and Fe^{2+} (0−0.8 mM) in SLF. (c) Yields of carbon- (yellow) and oxygen-centered (blue) organic radicals from isoprene SOA in SLF as a function of $[Fe^{2+}]/[ISO]$ molar ratios. The markers are experimental data. The solid lines represent the best fits of the kinetic model and the shaded areas represent the modeling uncertainties. (d) Organic radical yields (BMPO−R + BMPO−OR) versus total peroxide molar fractions in isoprene, α-terpineol, and toluene SOA with 0 (square) or 0.4 mM (circle) Fe^{2+}. The color scale represents the DTT consumption rate normalized by SOA mass (DTTm). The error bars in all panels represent the error propagation from the two duplicates in EPR measurement or total peroxide measurement and the uncertainty in SOA mass measurements.

of catalytic and redox reactions between Fe^{3+} and ascorbate particularly under different pH.

Overall, the implemented mechanisms successfully reproduce the time dependence of organic radical formation (Figure 4a,b) as well as the concentration dependence (Figure 4c), demonstrating the consistency of model simulations with experiments. We measured peroxide molar fractions in SOA, showing a positive correlation with organic radical yields by SOA in the presence of Fe^{2+} (circles in Figure 4d). It indicates that peroxides (ROOR + ROOH) are highly probable sources of aqueous organic radical formation. This is in line with a very recent study showing that the total ROS production from cooking SOA can be enhanced substantially through atmospheric aging, coinciding with the elevation in peroxide contents.[59] Isoprene SOA is measured to have high peroxide content (~97%) compared to Surratt et al.[60] (~61%, from a Teflon chamber); this difference may be due to excess $RO_2^\bullet$ chemistry in the PAM reactor, inducing more production of peroxides through termination steps such as $RO_2^\bullet + HO_2^\bullet \rightarrow ROOH$ and $RO_2^\bullet + RO_2^\bullet \rightarrow ROOR$.[4] Toluene SOA has the lowest peroxide content with 18%, which is consistent with a previous study,[61] leading to a lower organic radical yield.

To investigate the linkage between organic radical formation and oxidative potential, we performed the DTT assay on mixtures of SOA and Fe^{2+} and the results are shown by the color scale in Figure 4d (see also Table S3). The DTT consumption rates normalized by SOA mass (DTTm) for isoprene SOA (33.4 ± 6.2 pmol min^{-1} μg^{-1}) and toluene SOA (22.3 ± 2.5 pmol min^{-1} μg^{-1}) are consistent with previous studies.[62,63] With Fe^{2+} addition, clear enhancements of DTTm are observed for all types of SOA. Due to the moderate DTT activity from Fe^{2+} alone (Figure S6), SOA and Fe^{2+} demonstrate a strong synergistic effect in causing oxidative potential (Table S3). Figure 4d shows no clear association between organic radical yields and DTTm. Despite the lowest organic radical yields from mixtures of toluene SOA and Fe^{2+}, they induce relatively high DTTm (42.8 ± 0.4 pmol min^{-1} μg^{-1}), which is comparable with mixtures of isoprene SOA and Fe^{2+} (49.0 ± 11.2 pmol min^{-1} μg^{-1}). Tuet et al.[64] reported generally higher DTT activities from anthropogenic SOA than biogenic SOA, although the interactions of SOA and transition

https://doi.org/10.1021/acs.est.1c04334
Environ. Sci. Technol. XXXX, XXX, XXX−XXX

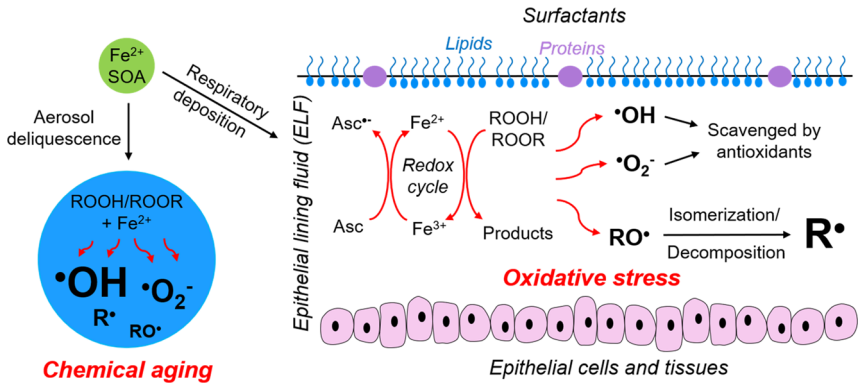

Figure 5. Implications of free radical formation by SOA and Fe^{2+} in water and epithelial lining fluid. Ambient aerosol particles containing SOA and Fe^{2+} can undergo deliquescence and release ROS dominated by $^{\bullet}OH$ and $O_2^{\bullet-}/HO_2^{\bullet}$ through Fe^{2+}-facilitated decomposition of organic hydroperoxides and subsequent aqueous reactions. Upon respiratory deposition, various radical species can be generated by interactions of ROOH/ROOR, Fe^{2+}, and antioxidants. $^{\bullet}OH$ and $O_2^{\bullet-}/HO_2^{\bullet}$ can be effectively scavenged by antioxidants, which may contribute to antioxidant depletion. The organic radical formation dominated by $R^{\bullet}$ with relatively long lifetimes may trigger lipid peroxidation to cause oxidative stress.

metals in oxidative potential are still understudied. Dedicated studies are necessary to further elucidate the link between ROS formation and oxidative potential from SOA.

Implications. This work establishes the mechanisms driving organic radical formation by the interactions among SOA, Fe^{2+} in SLF as shown in Figure 5. In liquid droplets formed through aerosol deliquescence, the decomposition of organic hydroperoxides in SOA can be promoted by Fe^{2+}, leading to enhanced formation of $^{\bullet}OH$ and $O_2^{\bullet-}/HO_2^{\bullet}$ with a minor contribution from organic radicals (R1−R4). These aqueous-phase processes involving ROS formation are efficient pathways for the chemical aging of SOA,[65,66] which may lead to the change of particle properties such as cloud condensation nuclei activity[67] and optical properties.[68]

Upon respiratory deposition of aerosol particles, SOA and Fe^{2+} may interact and release various radical species in epithelial lining fluid (ELF). While organic peroxides are thermally stable under physiological temperature,[69] the chemical lifetimes of organic peroxides with respect to Fe^{2+} reactions are calculated to be 0.3−46 h depending on Fe^{2+} concentrations in the experimental range of 0.05−0.8 mM. Meanwhile, the antioxidant defense system can counteract ROS formation: for example, ascorbate efficiently scavenges $^{\bullet}OH$ and $O_2^{\bullet-}/HO_2^{\bullet}$ with relatively fast rate constants of ∼1.8 × 10^{-11} cm^{-3} s^{-1} and ∼3.6 × 10^{-16} cm^{-3} s^{-1}, respectively.[70,71] In comparison, organic radicals, especially $R^{\bullet}$, react with ascorbate more slowly by multiple orders of magnitude, leading to much longer lifetimes.[54] A recent study characterized that the reaction rates of ascorbate and glutathione with alkyl radicals are too slow to protect proteins from peroxidation.[72] The rapid redox cycling of Fe^{3+}/Fe^{2+} maintained by ascorbate can further facilitate the ROOR decomposition and subsequent organic radical formation (R5, R10−R14, R63). Note that Fe^{3+}/Fe^{2+} redox cycles can also be mediated by ROS such as superoxide,[44,73] which can be hindered by the addition of antioxidants through direct scavenging of ROS. Antioxidants play a reciprocal role by depleting short-lived reactive radicals while amplifying organic radical formation.

Epithelial cell membranes contain phospholipid bilayers and $^{\bullet}OH$ and $HO_2^{\bullet}$ are known to initiate a cascade of propagation reactions of lipid peroxidation,[74,75] which may alter the membrane fluidity and trigger the inactivation of membrane-embedded proteins functioning as ion channels and receptors.[76] Our results on persistency of organic radicals even in the presence of antioxidants imply that organic radicals may also participate in radical chain reactions to be involved in lipid peroxidation. Despite the significance in numerous pathological processes, lipid peroxidation has not been linked mechanistically to radical formation from organic aerosols and transition metals, which underlines the need of future studies. Overall, our experimental and modeling results demonstrate the central role of Fe^{2+} in inducing organic radical formation by facilitating ROOR decomposition in lung fluid, highlighting the significance of the interactions among redox-active components in ambient PM in potentially causing oxidative stress.

■ ASSOCIATED CONTENT

Supporting Information

The Supporting Information is available free of charge at https://pubs.acs.org/doi/10.1021/acs.est.1c04334.

Additional discussion on reaction mechanisms and peroxide measurements; chemical reactions and parameters in the kinetic model; molar fractions of ROOH, R_1R_2CHOH and ROOR in isoprene SOA; Mass normalized DTT consumption rate by SOA and Fe^{2+}; calibration curves of ferrozine method and peroxide measurement; deconvoluted EPR spectra from isoprene SOA and Fe^{2+} in water and SLF; EPR spectra of Fenton system; EPR spectra of α-terpineol and toluene SOA in water and SLF; DTT consumption rates of SOA and Fe^{2+} (PDF)

■ AUTHOR INFORMATION

Corresponding Author

Manabu Shiraiwa − *Department of Chemistry, University of California, Irvine, California 92697-2025, United States;* orcid.org/0000-0003-2532-5373; Email: m.shiraiwa@uci.edu

Authors

Jinlai Wei − *Department of Chemistry, University of California, Irvine, California 92697-2025, United States;* orcid.org/0000-0002-4741-9015

https://doi.org/10.1021/acs.est.1c04334
Environ. Sci. Technol. XXXX, XXX, XXX−XXX

Ting Fang − *Department of Chemistry, University of California, Irvine, California 92697-2025, United States;* orcid.org/0000-0002-4845-2749

Pascale S. J. Lakey − *Department of Chemistry, University of California, Irvine, California 92697-2025, United States;* orcid.org/0000-0003-2923-4073

Complete contact information is available at: https://pubs.acs.org/10.1021/acs.est.1c04334

Notes

The authors declare no competing financial interest.

■ ACKNOWLEDGMENTS

The research described in this article was conducted under contract to the Health Effects Institute (HEI) (Walter A. Rosenblith New Investigator Award, no. 4964-RFA17-3/18-6), an organization jointly funded by the United States Environmental Protection Agency (EPA) (Assistance Award no. CR-83590201) and certain motor vehicle and engine manufacturers. The contents of this article neither necessarily reflect the views of HEI, or its sponsors, nor do they necessarily reflect the views and policies of the EPA or motor vehicle and engine manufacturers. We also acknowledge funding from the National Science Foundation (CHE-1808125). We acknowledge Prof. William Brune (Pennsylvania State University) for loaning the PAM reactor and Dr. Thomas Berkemeier (Max Planck Institute for Chemistry) for sharing the code of Monte Carlo genetic algorithm.

■ REFERENCES

(1) Jimenez, J. L.; Canagaratna, M. R.; Donahue, N. M.; Prevot, A. S. H.; Zhang, Q.; Kroll, J. H.; DeCarlo, P. F.; Allan, J. D.; Coe, H.; Ng, N. L.; Aiken, A. C.; Docherty, K. S.; Ulbrich, I. M.; Grieshop, A. P.; Robinson, A. L.; Duplissy, J.; Smith, J. D.; Wilson, K. R.; Lanz, V. A.; Hueglin, C.; Sun, Y. L.; Tian, J.; Laaksonen, A.; Raatikainen, T.; Rautiainen, J.; Vaattovaara, P.; Ehn, M.; Kulmala, M.; Tomlinson, J. M.; Collins, D. R.; Cubison, M. J.; Dunlea, E. J.; Huffman, J. A.; Onasch, T. B.; Alfarra, M. R.; Williams, P. I.; Bower, K.; Kondo, Y.; Schneider, J.; Drewnick, F.; Borrmann, S.; Weimer, S.; Demerjian, K.; Salcedo, D.; Cottrell, L.; Griffin, R.; Takami, A.; Miyoshi, T.; Hatakeyama, S.; Shimono, A.; Sun, J. Y.; Zhang, Y. M.; Dzepina, K.; Kimmel, J. R.; Sueper, D.; Jayne, J. T.; Herndon, S. C.; Trimborn, A. M.; Williams, L. R.; Wood, E. C.; Middlebrook, A. M.; Kolb, C. E.; Baltensperger, U.; Worsnop, D. R. Evolution of organic aerosols in the atmosphere. *Science* **2009**, *326* (5959), 1525−1529.

(2) Shrivastava, M.; Cappa, C. D.; Fan, J. W.; Goldstein, A. H.; Guenther, A. B.; Jimenez, J. L.; Kuang, C.; Laskin, A.; Martin, S. T.; Ng, N. L.; Petaja, T.; Pierce, J. R.; Rasch, P. J.; Roldin, P.; Seinfeld, J. H.; Shilling, J.; Smith, J. N.; Thornton, J. A.; Volkamer, R.; Wang, J.; Worsnop, D. R.; Zaveri, R. A.; Zelenyuk, A.; Zhang, Q. Recent advances in understanding secondary organic aerosol: Implications for global climate forcing. *Rev. Geophys.* **2017**, *55* (2), 509−559.

(3) Shiraiwa, M.; Ueda, K.; Pozzer, A.; Lammel, G.; Kampf, C. J.; Fushimi, A.; Enami, S.; Arangio, A. M.; Frohlich-Nowoisky, J.; Fujitani, Y.; Furuyama, A.; Lakey, P. S. J.; Lelieveld, J.; Lucas, K.; Morino, Y.; Poschl, U.; Takaharna, S.; Takami, A.; Tong, H. J.; Weber, B.; Yoshino, A.; Sato, K. Aerosol Health Effects from Molecular to Global Scales. *Environ. Sci. Technol.* **2017**, *51* (23), 13545−13567.

(4) Ziemann, P. J.; Atkinson, R. Kinetics, products, and mechanisms of secondary organic aerosol formation. *Chem. Soc. Rev.* **2012**, *41* (19), 6582−6605.

(5) de Kok, T. M. C. M.; Driece, H. A. L.; Hogervorst, J. G. F.; Briedé, J. J. Toxicological assessment of ambient and traffic-related particulate matter: A review of recent studies. *Mutat. Res., Rev. Mutat. Res.* **2006**, *613* (2), 103−122.

(6) Grigoratos, T.; Martini, G. Brake wear particle emissions: a review. *Environ. Sci. Pollut. Res.* **2015**, *22* (4), 2491−2504.

(7) Fang, T.; Guo, H.; Verma, V.; Peltier, R. E.; Weber, R. J. PM2.5 water-soluble elements in the southeastern United States: automated analytical method development, spatiotemporal distributions, source apportionment, and implications for heath studies. *Atmos. Chem. Phys.* **2015**, *15* (20), 11667−11682.

(8) Majestic, B. J.; Schauer, J. J.; Shafer, M. M. Application of synchrotron radiation for measurement of iron red-ox speciation in atmospherically processed aerosols. *Atmos. Chem. Phys.* **2007**, *7* (10), 2475−2487.

(9) Kieber, R. J.; Skrabal, S. A.; Smith, B. J.; Willey, J. D. Organic Complexation of Fe(II) and Its Impact on the Redox Cycling of Iron in Rain. *Environ. Sci. Technol.* **2005**, *39* (6), 1576−1583.

(10) Usher, C. R.; Michel, A. E.; Grassian, V. H. Reactions on Mineral Dust. *Chem. Rev.* **2003**, *103* (12), 4883−4940.

(11) Fang, T.; Guo, H.; Verma, V.; Peltier, R. E.; Weber, R. J. PM2.5 water-soluble elements in the southeastern United States: automated analytical method development, spatiotemporal distributions, source apportionment, and implications for heath studies. *Atmos. Chem. Phys.* **2015**, *15* (20), 11667−11682.

(12) Bondy, A. L.; Bonanno, D.; Moffet, R. C.; Wang, B.; Laskin, A.; Ault, A. P. The diverse chemical mixing state of aerosol particles in the southeastern United States. *Atmos. Chem. Phys.* **2018**, *18* (16), 12595−12612.

(13) Fang, T.; Guo, H.; Verma, V.; Peltier, R. E.; Weber, R. J. PM2.5 water-soluble elements in the southeastern United States: automated analytical method development, spatiotemporal distributions, source apportionment, and implications for heath studies. *Atmos. Chem. Phys.* **2015**, *15*.201166711682

(14) Saffari, A.; Daher, N.; Shafer, M. M.; Schauer, J. J.; Sioutas, C. Global Perspective on the Oxidative Potential of Airborne Particulate Matter: A Synthesis of Research Findings. *Environ. Sci. Technol.* **2014**, *48* (13), 7576−7583.

(15) Daellenbach, K. R.; Uzu, G.; Jiang, J.; Cassagnes, L.-E.; Leni, Z.; Vlachou, A.; Stefenelli, G.; Canonaco, F.; Weber, S.; Segers, A.; Kuenen, J. J. P.; Schaap, M.; Favez, O.; Albinet, A.; Aksoyoglu, S.; Dommen, J.; Baltensperger, U.; Geiser, M.; El Haddad, I.; Jaffrezo, J.-L.; Prévôt, A. S. H. Sources of particulate-matter air pollution and its oxidative potential in Europe. *Nature* **2020**, *587* (7834), 414−419.

(16) Ehn, M.; Thornton, J. A.; Kleist, E.; Sipila, M.; Junninen, H.; Pullinen, I.; Springer, M.; Rubach, F.; Tillmann, R.; Lee, B.; Lopez-Hilfiker, F.; Andres, S.; Acir, I. H.; Rissanen, M.; Jokinen, T.; Schobesberger, S.; Kangasluoma, J.; Kontkanen, J.; Nieminen, T.; Kurten, T.; Nielsen, L. B.; Jorgensen, S.; Kjaergaard, H. G.; Canagaratna, M.; Dal Maso, M.; Berndt, T.; Petaja, T.; Wahner, A.; Kerminen, V. M.; Kulmala, M.; Worsnop, D. R.; Wildt, J.; Mentel, T. F. A large source of low-volatility secondary organic aerosol. *Nature* **2014**, *506* (7489), 476−479.

(17) Bianchi, F.; Kurten, T.; Riva, M.; Mohr, C.; Rissanen, M. P.; Roldin, P.; Berndt, T.; Crounse, J. D.; Wennberg, P. O.; Mentel, T. F.; Wildt, J.; Junninen, H.; Jokinen, T.; Kulmala, M.; Worsnop, D. R.; Thornton, J. A.; Donahue, N.; Kjaergaard, H. G.; Ehn, M. Highly Oxygenated Organic Molecules (HOM) from Gas-Phase Autoxidation Involving Peroxy Radicals: A Key Contributor to Atmospheric Aerosol. *Chem. Rev.* **2019**, *119* (6), 3472−3509.

(18) Krapf, M.; El Haddad, I.; Bruns, E. A.; Molteni, U.; Daellenbach, K. R.; Prevot, A. S. H.; Baltensperger, U.; Dommen, J. Labile Peroxides in Secondary Organic Aerosol. *Chem-Us* **2016**, *1* (4), 603−616.

(19) Tong, H.; Arangio, A. M.; Lakey, P. S. J.; Berkemeier, T.; Liu, F. B.; Kampf, C. J.; Brune, W. H.; Poschl, U.; Shiraiwa, M. Hydroxyl radicals from secondary organic aerosol decomposition in water. *Atmos. Chem. Phys.* **2016**, *16* (3), 1761−1771.

(20) Tong, H. J.; Zhang, Y.; Filippi, A.; Wang, T.; Li, C. P.; Liu, F. B.; Leppla, D.; Kourtchev, I.; Wang, K.; Keskinen, H. M.; Levula, J. T.; Arangio, A. M.; Shen, F. X.; Ditas, F.; Martin, S. T.; Artaxo, P.;

Godoi, R. H. M.; Yamamoto, C. I.; de Souza, R. A. F.; Huang, R. J.; Berkemeier, T.; Wang, Y. S.; Su, H.; Cheng, Y. F.; Pope, F. D.; Fu, P. Q.; Yao, M. S.; Pohlker, C.; Petaja, T.; Kulmala, M.; Andreae, M. O.; Shiraiwa, M.; Poschl, U.; Hoffmann, T.; Kalberer, M. Radical Formation by Fine Particulate Matter Associated with Highly Oxygenated Molecules. *Environ. Sci. Technol.* **2019**, *53* (21), 12506−12518.

(21) Paulson, S. E.; Gallimore, P. J.; Kuang, X. B. M.; Chen, J. R.; Kalberer, M.; Gonzalez, D. H. A light-driven burst of hydroxyl radicals dominates oxidation chemistry in newly activated cloud droplets. *Sci. Adv.* **2019**, *5* (5), 1−7.

(22) Tuet, W. Y.; Chen, Y.; Fok, S.; Gao, D.; Weber, R. J.; Champion, J. A.; Ng, N. L. Chemical and cellular oxidant production induced by naphthalene secondary organic aerosol (SOA): effect of redox-active metals and photochemical aging. *Sci. Rep.* **2017**, *7* (1), 15157.

(23) Wei, J.; Fang, T.; Wong, C.; Lakey, P. S. J.; Nizkorodov, S. A.; Shiraiwa, M. Superoxide Formation from Aqueous Reactions of Biogenic Secondary Organic Aerosols. *Environ. Sci. Technol.* **2021**, *55* (1), 260−270.

(24) Alpert, P. A.; Dou, J.; Corral Arroyo, P.; Schneider, F.; Xto, J.; Luo, B.; Peter, T.; Huthwelker, T.; Borca, C. N.; Henzler, K. D.; Schaefer, T.; Herrmann, H.; Raabe, J.; Watts, B.; Krieger, U. K.; Ammann, M. Photolytic radical persistence due to anoxia in viscous aerosol particles. *Nat. Commun.* **2021**, *12* (1), 1769.

(25) Kang, E.; Root, M. J.; Toohey, D. W.; Brune, W. H. Introducing the concept of Potential Aerosol Mass (PAM). *Atmos. Chem. Phys.* **2007**, *7* (22), 5727−5744.

(26) Guenther, A. B.; Jiang, X.; Heald, C. L.; Sakulyanontvittaya, T.; Duhl, T.; Emmons, L. K.; Wang, X. The Model of Emissions of Gases and Aerosols from Nature version 2.1 (MEGAN2.1): an extended and updated framework for modeling biogenic emissions. *Geosci. Model Dev.* **2012**, *5* (6), 1471−1492.

(27) Piccot, S. D.; Watson, J. J.; Jones, J. W. A global inventory of volatile organic compound emissions from anthropogenic sources. *Journal of Geophysical Research: Atmospheres* **1992**, *97* (D9), 9897−9912.

(28) Nazaroff, W. W.; Weschler, C. J. Cleaning products and air fresheners: exposure to primary and secondary air pollutants. *Atmos. Environ.* **2004**, *38* (18), 2841−2865.

(29) Lambe, A. T.; Chhabra, P. S.; Onasch, T. B.; Brune, W. H.; Hunter, J. F.; Kroll, J. H.; Cummings, M. J.; Brogan, J. F.; Parmar, Y.; Worsnop, D. R.; Kolb, C. E.; Davidovits, P. Effect of oxidant concentration, exposure time, and seed particles on secondary organic aerosol chemical composition and yield. *Atmos. Chem. Phys.* **2015**, *15* (6), 3063−3075.

(30) Lambe, A. T.; Ahern, A. T.; Williams, L. R.; Slowik, J. G.; Wong, J. P. S.; Abbatt, J. P. D.; Brune, W. H.; Ng, N. L.; Wright, J. P.; Croasdale, D. R.; Worsnop, D. R.; Davidovits, P.; Onasch, T. B. Characterization of aerosol photooxidation flow reactors: heterogeneous oxidation, secondary organic aerosol formation and cloud condensation nuclei activity measurements. *Atmos. Meas. Tech.* **2011**, *4* (3), 445−461.

(31) Peng, Z.; Jimenez, J. L. Radical chemistry in oxidation flow reactors for atmospheric chemistry research. *Chem. Soc. Rev.* **2020**, *49* (9), 2570−2616.

(32) Brune, W. H. The Chamber Wall Index for Gas−Wall Interactions in Atmospheric Environmental Enclosures. *Environ. Sci. Technol.* **2019**, *53* (7), 3645−3652.

(33) Peng, Z.; Day, D. A.; Ortega, A. M.; Palm, B. B.; Hu, W. W.; Stark, H.; Li, R.; Tsigaridis, K.; Brune, W. H.; Jimenez, J. L. Non-OH chemistry in oxidation flow reactors for the study of atmospheric chemistry systematically examined by modeling. *Atmos. Chem. Phys.* **2016**, *16* (7), 4283−4305.

(34) Charrier, J. G.; Anastasio, C. Rates of Hydroxyl Radical Production from Transition Metals and Quinones in a Surrogate Lung Fluid. *Environ. Sci. Technol.* **2015**, *49* (15), 9317−9325.

(35) Charrier, J. G.; Anastasio, C. Impacts of antioxidants on hydroxyl radical production from individual and mixed transition metals in a surrogate lung fluid. *Atmos. Environ.* **2011**, *45* (40), 7555−7562.

(36) Wei, J.; Yu, H.; Wang, Y.; Verma, V. Complexation of Iron and Copper in Ambient Particulate Matter and Its Effect on the Oxidative Potential Measured in a Surrogate Lung Fluid. *Environ. Sci. Technol.* **2019**, *53* (3), 1661−1671.

(37) Docherty, K. S.; Wu, W.; Lim, Y. B.; Ziemann, P. J. Contributions of organic peroxides to secondary aerosol formed from reactions of monoterpenes with O_3. *Environ. Sci. Technol.* **2005**, *39* (11), 4049−4059.

(38) Awtrey, A. D.; Connick, R. E. The Absorption Spectra of I2, I3-, I-, IO3-, S4O6= and S2O3 = . Heat of the Reaction I3- = I2 + I. *J. Am. Chem. Soc.* **1951**, *73* (4), 1842−1843.

(39) Fang, T.; Verma, V.; Guo, H.; King, L. E.; Edgerton, E. S.; Weber, R. J. A semi-automated system for quantifying the oxidative potential of ambient particles in aqueous extracts using the dithiothreitol (DTT) assay: results from the Southeastern Center for Air Pollution and Epidemiology (SCAPE). *Atmos. Meas. Tech.* **2015**, *8* (1), 471−482.

(40) Goldstein, S.; Meyerstein, D. Comments on the mechanism of the ″Fenton like″ reaction. *Acc. Chem. Res.* **1999**, *32* (7), 547−550.

(41) Gilbert, B. C.; Holmes, R. G.; Laue, H. A.; Norman, R. O. Electron spin resonance studies. Part L. Reactions of alkoxyl radicals generated from alkyl hydroperoxides and titanium (III) ion in aqueous solution. *J. Chem. Soc., Perkin Trans. 2* **1976**, *9*, 1047−1052.

(42) Erben-Russ, M.; Michel, C.; Bors, W.; Saran, M. Absolute rate constants of alkoxyl radical reactions in aqueous solution. *J. Phys. Chem.* **1987**, *91* (9), 2362−2365.

(43) Carrasquillo, A. J.; Daumit, K. E.; Kroll, J. H. Radical Reactivity in the Condensed Phase: Intermolecular versus Intramolecular Reactions of Alkoxy Radicals. *J. Phys. Chem. Lett.* **2015**, *6* (12), 2388−2392.

(44) Gonzalez, D. H.; Cala, C. K.; Peng, Q.; Paulson, S. E. HULIS Enhancement of Hydroxyl Radical Formation from Fe(II): Kinetics of Fulvic Acid−Fe(II) Complexes in the Presence of Lung Antioxidants. *Environ. Sci. Technol.* **2017**, *51* (13), 7676−7685.

(45) Docherty, K. S.; Wu, W.; Lim, Y. B.; Ziemann, P. J. Contributions of organic peroxides to secondary aerosol formed from reactions of monoterpenes with O_3. *Environ. Sci. Technol.* **2005**, *39* (11), 4049−4059.

(46) Buettner, G. R.; Jurkiewicz, B. A. Ascorbate free radical as a marker of oxidative stress: An EPR study. *Free Radical Biol. Med.* **1993**, *14* (1), 49−55.

(47) Qiu, J.; Liang, Z.; Tonokura, K.; Colussi, A. J.; Enami, S. Stability of Monoterpene-Derived α-Hydroxyalkyl-Hydroperoxides in Aqueous Organic Media: Relevance to the Fate of Hydroperoxides in Aerosol Particle Phases. *Environ. Sci. Technol.* **2020**, *54* (7), 3890−3899.

(48) Enami, S. Fates of Organic Hydroperoxides in Atmospheric Condensed Phases. *J. Phys. Chem. A* **2021**, *125* (21), 4513−4523.

(49) Herrmann, H.; Tilgner, A.; Barzaghi, P.; Majdik, Z.; Gligorovski, S.; Poulain, L.; Monod, A. Towards a more detailed description of tropospheric aqueous phase organic chemistry: CAPRAM 3.0. *Atmos. Environ.* **2005**, *39* (23−24), 4351−4363.

(50) Denisov, E. T.; Tumanov, V. E. Estimation of the bond dissociation energies from the kinetic characteristics of liquid-phase radical reactions. *Russ. Chem. Rev.* **2005**, *74* (9), 825−858.

(51) Eames, J.; Watkinson, M. Catalytic Allylic Oxidation of Alkenes Using an Asymmetric Kharasch−Sosnovsky Reaction. *Angew. Chem., Int. Ed.* **2001**, *40* (19), 3567−3571.

(52) Studer, A.; Curran, D. P. Catalysis of Radical Reactions: A Radical Chemistry Perspective. *Angew. Chem., Int. Ed.* **2016**, *55* (1), 58−102.

(53) Chevallier, E.; Jolibois, R. D.; Meunier, N.; Carlier, P.; Monod, A. Fenton-like" reactions of methylhydroperoxide and ethylhydroperoxide with Fe2+ in liquid aerosols under tropospheric conditions. *Atmos. Environ.* **2004**, *38* (6), 921−933.

https://doi.org/10.1021/acs.est.1c04334
Environ. Sci. Technol. XXXX, XXX, XXX−XXX

(54) Buettner, G. R.; Jurkiewicz, B. A. Catalytic metals, ascorbate and free radicals: combinations to avoid. *Radiat. Res.* **1996**, *145* (5), 532−541.
(55) Lakey, P. S. J.; Berkemeier, T.; Tong, H. J.; Arangio, A. M.; Lucas, K.; Poschl, U.; Shiraiwa, M. Chemical exposure-response relationship between air pollutants and reactive oxygen species in the human respiratory tract. *Sci. Rep.* **2016**, *6*, 1−6.
(56) Sun, H.; Xie, G.; He, D.; Zhang, L. Ascorbic acid promoted magnetite Fenton degradation of alachlor: Mechanistic insights and kinetic modeling. *Appl. Catal., B* **2020**, *267*, 118383.
(57) Valko, M.; Morris, H.; Cronin, M. T. D. Metals, toxicity and oxidative stress. *Curr. Med. Chem.* **2005**, *12* (10), 1161−1208.
(58) Shen, J.; Griffiths, P. T.; Campbell, S. J.; Utinger, B.; Kalberer, M.; Paulson, S. E. Ascorbate oxidation by iron, copper and reactive oxygen species: review, model development, and derivation of key rate constants. *Sci. Rep.* **2021**, *11* (1), 7417.
(59) Wang, S.; Takhar, M.; Zhao, Y.; Al Rashdi, L. N. S.; Chan, A. W. H. Dynamic Oxidative Potential of Organic Aerosol from Heated Cooking Oil. *Acs Earth Space Chem.* **2021**, *5* (5), 1150−1162.
(60) Surratt, J. D.; Murphy, S. M.; Kroll, J. H.; Ng, N. L.; Hildebrandt, L.; Sorooshian, A.; Szmigielski, R.; Vermeylen, R.; Maenhaut, W.; Claeys, M. Chemical composition of secondary organic aerosol formed from the photooxidation of isoprene. *J. Phys. Chem. A* **2006**, *110* (31), 9665−9690.
(61) Sato, K.; Hatakeyama, S.; Imamura, T. Secondary Organic Aerosol Formation during the Photooxidation of Toluene: NOx Dependence of Chemical Composition. *J. Phys. Chem. A* **2007**, *111* (39), 9796−9808.
(62) Jiang, H.; Jang, M.; Sabo-Attwood, T.; Robinson, S. E. Oxidative potential of secondary organic aerosols produced from photooxidation of different hydrocarbons using outdoor chamber under ambient sunlight. *Atmos. Environ.* **2016**, *131*, 382−389.
(63) Fujitani, Y.; Furuyama, A.; Tanabe, K.; Hirano, S. Comparison of Oxidative Abilities of PM2.5 Collected at Traffic and Residential Sites in Japan. Contribution of Transition Metals and Primary and Secondary Aerosols. *Aerosol Air Qual. Res.* **2017**, *17* (2), 574−587.
(64) Tuet, W. Y.; Chen, Y. L.; Xu, L.; Fok, S.; Gao, D.; Weber, R. J.; Ng, N. L. Chemical oxidative potential of secondary organic aerosol (SOA) generated from the photooxidation of biogenic and anthropogenic volatile organic compounds. *Atmos. Chem. Phys.* **2017**, *17* (2), 839−853.
(65) Herrmann, H.; Schaefer, T.; Tilgner, A.; Styler, S. A.; Weller, C.; Teich, M.; Otto, T. Tropospheric Aqueous-Phase Chemistry: Kinetics, Mechanisms, and Its Coupling to a Changing Gas Phase. *Chem. Rev.* **2015**, *115* (10), 4259−4334.
(66) McNeill, V. F. Aqueous Organic Chemistry in the Atmosphere: Sources and Chemical Processing of Organic Aerosols. *Environ. Sci. Technol.* **2015**, *49* (3), 1237−1244.
(67) Farmer, D. K.; Cappa, C. D.; Kreidenweis, S. M. Atmospheric Processes and Their Controlling Influence on Cloud Condensation Nuclei Activity. *Chem. Rev.* **2015**, *115* (10), 4199−4217.
(68) Laskin, A.; Laskin, J.; Nizkorodov, S. A. Chemistry of Atmospheric Brown Carbon. *Chem. Rev.* **2015**, *115* (10), 4335−4382.
(69) Sanchez, J.; Myers, T. N. Peroxides and peroxide compounds, organic peroxides. *Kirk-Othmer encyclopedia of chemical technology* **2000**, 1−86.
(70) Adams, G.; Boag, J.; Currant, J.; Michael, B. *Absolute Rate Constants for the Reaction of the Hydroxyl Radical with Organic Compounds.*; Academic Press: New York, 1965; p 13.
(71) Nadezhdin, A. D.; Dunford, H. B. The oxidation of ascorbic acid and hydroquinone by perhydroxyl radicals. A flash photolysis study. *Can. J. Chem.* **1979**, *57* (23), 3017−3022.
(72) Nauser, T.; Gebicki, J. M. Reaction rates of glutathione and ascorbate with alkyl radicals are too slow for protection against protein peroxidation in vivo. *Arch. Biochem. Biophys.* **2017**, *633*, 118−123.
(73) Voelker, B. M.; Sedlak, D. L. Iron reduction by photoproduced superoxide in seawater. *Mar. Chem.* **1995**, *50* (1), 93−102.
(74) Ayala, A.; Muñoz, M. F.; Argüelles, S. Lipid Peroxidation: Production, Metabolism, and Signaling Mechanisms of Malondialdehyde and 4-Hydroxy-2-Nonenal. *Oxid. Med. Cell. Longevity* **2014**, *2014*, 360438.
(75) Yin, H.; Xu, L.; Porter, N. A. Free Radical Lipid Peroxidation: Mechanisms and Analysis. *Chem. Rev.* **2011**, *111* (10), 5944−5972.
(76) Los, D. A.; Murata, N. Membrane fluidity and its roles in the perception of environmental signals. *Biochim. Biophys. Acta, Biomembr.* **2004**, *1666* (1), 142−157.

https://doi.org/10.1021/acs.est.1c04334
Environ. Sci. Technol. XXXX, XXX, XXX−XXX